2009

Problems in synthetic-aperture radar imaging

Cheney, Margaret

Inverse Problems, Volume 25, (2009)
http://hdl.handle.net/10945/43818

Inverse Problems **25** (2009) 123005 (18pp) doi:10.1088/0266-5611/25/12/123005

TOPICAL REVIEW

Problems in synthetic-aperture radar imaging

Margaret Cheney[1] **and Brett Borden**[2]

[1] Department of Mathematical Sciences, Rensselaer Polytechnic Institute, Troy, NY 12180, USA
[2] Physics Department, Naval Postgraduate School, Monterey, CA 93943, USA

Received 1 June 2009, in final form 6 August 2009
Published 23 November 2009
Online at stacks.iop.org/IP/25/123005

Abstract
The purpose of this review is to explain the basics of synthetic-aperture radar imaging to the *Inverse Problems* audience, and to list a variety of associated open problems.

(Some figures in this article are in colour only in the electronic version)

1. Introduction

'Radar' is an acronym for RAdio Detection And Ranging. Radar was originally developed [6, 12, 87, 91, 102] as a technique for detecting objects and determining their positions by means of *echo-location*, and this remains the principal function of modern radar systems. However, radar systems have evolved over more than seven decades to perform a variety of very complex functions; one such function is imaging [16, 28–30, 36, 40, 49, 59, 79, 84].

Radar-based imaging is a technology that has been developed mainly within the engineering community. There are good reasons for this: some of the critical challenges are (1) transmitting microwave energy at high power, (2) detecting microwave energy, and (3) interpreting and extracting information from the received signals. The first two problems have to do with the development of appropriate hardware; however, these problems have now largely been solved, although there is ongoing work to make the hardware smaller and lighter. The third problem is essentially a set of mathematical challenges, and this is the area where most of the current effort is taking place.

Existing imaging methods rely on very specific simplifying assumptions about radar scattering phenomenology and data collection scenarios:

(i) They assume that the target or scene behaves as a rigid body. This assumption is obviously inadequate for scenes that include multiple moving objects.
(ii) They also assume a linear relationship between the data and scene. In many situations, this is also inadequate.

Moreover, the process of extracting information from radar imagery is incompletely developed.

The purpose of this review is to explain the basics of synthetic-aperture radar imaging to the *Inverse Problems* audience, and to list a variety of associated open problems. In

section 2, we outline a model for radar propagation and scattering, making the commonly used approximations. In sections 3 and 4, we show how synthetic apertures can be constructed and used in the problem of radar imaging. Section 5 is a listing of open problems.

2. Radar scattering

Most imaging radar systems make use of the *start–stop approximation* [40], in which the sensor and scattering object (target) are assumed to be stationary during the time interval during which the pulse washes over the target. Thus the present discussion considers only scattering from stationary targets.

2.1. Scalar waves

We consider the case in which the region between the sensors and the scattering objects ('targets') consists of a homogeneous, lossless, non-dispersive atmosphere. In this situation, Maxwell's equations can be used [48] to obtain an inhomogeneous wave equation for the electric field $\boldsymbol{\mathcal{E}}$:

$$\nabla^2 \boldsymbol{\mathcal{E}}(t, \boldsymbol{x}) - \frac{1}{c^2} \frac{\partial^2 \boldsymbol{\mathcal{E}}(t, \boldsymbol{x})}{\partial t^2} = \boldsymbol{s}(t, \boldsymbol{x}) \tag{1}$$

and a similar equation for the magnetic field $\boldsymbol{\mathcal{B}}$. Here c denotes the speed of propagation of the wave in vacuum (which, for most remote sensing situations, is a good approximation to the speed in the atmosphere) and $\boldsymbol{s}$ is a source term that, in general, can involve $\boldsymbol{\mathcal{E}}$ and $\boldsymbol{\mathcal{B}}$. This source term is discussed in more detail below.

For simplicity we consider only one Cartesian component of equation (1):

$$\left(\nabla^2 - \frac{1}{c^2} \frac{\partial^2}{\partial t^2}\right) \mathcal{E}(t, \boldsymbol{x}) = s(t, \boldsymbol{x}), \tag{2}$$

where we have assumed atmospheric propagation between source and target.

2.2. Basic facts about the wave equation

A *fundamental solution* [93] of the wave equation is a generalized function [41, 93] satisfying

$$\left(\nabla^2 - \frac{1}{c^2} \frac{\partial^2}{\partial_t^2}\right) g(t, \boldsymbol{x}) = -\delta(t)\delta(\boldsymbol{x}). \tag{3}$$

The solution to (3) that is useful for us is

$$g(t, \boldsymbol{x}) = \frac{\delta(t - |\boldsymbol{x}|/c)}{4\pi |\boldsymbol{x}|} = \int \frac{\mathrm{e}^{-\mathrm{i}\omega(t-|\boldsymbol{x}|/c)}}{8\pi^2 |\boldsymbol{x}|} \, \mathrm{d}\omega, \tag{4}$$

where in the second equality we have used $\delta(t) = (1/2\pi) \int \exp(-\mathrm{i}\omega t) \, \mathrm{d}\omega$. The function $g(t, \boldsymbol{x})$ can be physically interpreted as the field at $(t, \boldsymbol{x})$ due to a source at the origin $\boldsymbol{x} = \boldsymbol{0}$ at time $t = 0$, and is called the *outgoing fundamental solution* or *(outgoing) Green's function*.

The Green's function [85] enables us to solve the constant-speed wave equation with *any* source term. In particular, the outgoing solution of

$$\left(\nabla^2 - \frac{1}{c^2} \frac{\partial^2}{\partial_t^2}\right) u(t, \boldsymbol{x}) = s(t, \boldsymbol{x}) \tag{5}$$

is

$$u(t, \boldsymbol{x}) = -\int g(t - t', \boldsymbol{x} - \boldsymbol{y}) s(t', \boldsymbol{y}) \, \mathrm{d}t' \, \mathrm{d}\boldsymbol{y}. \tag{6}$$

In the frequency domain, the equations corresponding to (3) and (4) are

$$(\nabla^2 + k^2)G = -\delta \qquad \text{and} \qquad G(\omega, \boldsymbol{x}) = \frac{\mathrm{e}^{\mathrm{i}k|\boldsymbol{x}|}}{4\pi|\boldsymbol{x}|}, \tag{7}$$

where the wave number k is defined as $k = \omega/c$.

2.3. Introduction to scattering theory

In radar problems, the source $\boldsymbol{s}$ is a sum of two terms, $\boldsymbol{s} = \boldsymbol{s}^{\mathrm{in}} + \boldsymbol{s}^{\mathrm{sc}}$, where $\boldsymbol{s}^{\mathrm{in}}$ models the transmitting antenna and $\boldsymbol{s}^{\mathrm{sc}}$ models the scattering object. The solution $\boldsymbol{\mathcal{E}}$, which we write as $\boldsymbol{\mathcal{E}}^{\mathrm{tot}}$, therefore splits into two parts: $\boldsymbol{\mathcal{E}}^{\mathrm{tot}} = \boldsymbol{\mathcal{E}}^{\mathrm{in}} + \boldsymbol{\mathcal{E}}^{\mathrm{sc}}$. The first term, $\boldsymbol{\mathcal{E}}^{\mathrm{in}}$, satisfies the wave equation for the known, prescribed source $\boldsymbol{s}^{\mathrm{in}}$. This part we call the *incident* field, because it is incident upon the scatterers. The second part of $\boldsymbol{\mathcal{E}}^{\mathrm{tot}}$ is due to target scattering, and this part is called the *scattered* field. In our simplified scalar model, we write $\mathcal{E}^{\mathrm{tot}} = \mathcal{E}^{\mathrm{in}} + \mathcal{E}^{\mathrm{sc}}$, where $\mathcal{E}^{\mathrm{in}}$ satisfies the wave equation for the known, prescribed source s^{in}.

One approach to finding the scattered field is to simply solve (2) directly, using for example numerical time-domain techniques. However, for many purposes, it is convenient to reformulate the scattering problem in terms of an integral equation.

2.3.1. The Lippmann–Schwinger integral equation. In scattering problems, the source term $\boldsymbol{s}^{\mathrm{sc}}$ (typically) represents the target's *response* to an incident field. This part of the source function will generally depend on the geometric and material properties of the target and on the form and strength of the incident field. Consequently, $\boldsymbol{s}^{\mathrm{sc}}$ can be quite complicated to describe analytically, and in general it will not have the same direction as $\boldsymbol{s}^{\mathrm{in}}$. Fortunately, for our purposes it is not necessary to provide a detailed analysis of the target's response; for stationary objects consisting of linear materials, we can write our scalar model s^{sc} as the time-domain convolution

$$s^{\mathrm{sc}}(t, \boldsymbol{x}) = -\int v(t - t', \boldsymbol{x})\mathcal{E}^{\mathrm{tot}}(t', \boldsymbol{x})\,\mathrm{d}t', \tag{8}$$

where $v(t, \boldsymbol{x})$ is called the reflectivity function. In the full vector case, v would be a matrix operating on the full vector $\boldsymbol{\mathcal{E}}^{\mathrm{tot}}$; here, we use only the single matrix element corresponding to the component considered in (2).

We can use (8) in (6) to express $\mathcal{E}^{\mathrm{sc}}$ in terms of the *Lippmann–Schwinger* integral equation [65]

$$\boxed{\mathcal{E}^{\mathrm{sc}}(t, \boldsymbol{x}) = \iint g(t - \tau, \boldsymbol{x} - \boldsymbol{z}) \int v(\tau - t', \boldsymbol{z})\mathcal{E}^{\mathrm{tot}}(t', \boldsymbol{z})\,\mathrm{d}t'\,\mathrm{d}\tau\mathrm{d}\boldsymbol{z}.} \tag{9}$$

2.3.2. The Lippmann–Schwinger equation in the frequency domain. In the frequency domain, the electric field and reflectivity function become

$$E(\omega, \boldsymbol{x}) = \int \mathrm{e}^{\mathrm{i}\omega t}\mathcal{E}(t, \boldsymbol{x})\,\mathrm{d}t \qquad \text{and} \qquad V(\omega, \boldsymbol{z}) = \int \mathrm{e}^{\mathrm{i}\omega t}v(t, \boldsymbol{z})\,\mathrm{d}t. \tag{10}$$

Thus the frequency-domain version of (1) is

$$\left(\nabla^2 + \frac{\omega^2}{c^2}\right)E(\omega, \boldsymbol{x}) = S(\omega, \boldsymbol{x}) \tag{11}$$

and of (9) is

$$E^{\mathrm{sc}}(\omega, \boldsymbol{x}) = -\int G(\omega, \boldsymbol{x} - \boldsymbol{z})V(\omega, \boldsymbol{z})E^{\mathrm{tot}}(\omega, \boldsymbol{z})\,\mathrm{d}\boldsymbol{z}. \tag{12}$$

The reflectivity function $V(\omega, \boldsymbol{x})$ can display a sensitive dependence on ω [48, 50, 72]. When the target is small in comparison with the wavelength of the incident field, for example, V is proportional to ω^2 (this behavior is known as 'Rayleigh scattering'). At higher frequencies (shorter wavelengths) the dependence on ω is typically less pronounced. In the so-called 'optical region', $V(\omega, \boldsymbol{x})$ is often approximated as being independent of ω (see, however, [77]); we use the optical approximation in this review and simply drop the ω dependence. In the time domain, this corresponds to $v(t, \boldsymbol{z}) = \delta(t)V(\boldsymbol{z})$, and the delta function allows us to carry out the t' integration in (9).

2.3.3. The Born approximation. For radar imaging, we measure $\mathcal{E}^{\text{sc}}$ at the antenna, and we would like to determine V from these measurements. However, both V and $\mathcal{E}^{\text{sc}}$ in the neighborhood of the target are unknown, and in (9) these unknowns are multiplied together. This nonlinearity makes it difficult to solve for V. Consequently, almost all work on radar imaging involves making the *Born* approximation, which is also known as the *weak-scattering* or *single-scattering* approximation [55, 65]. The Born approximation replaces $\mathcal{E}^{\text{tot}}$ on the right-hand side of (9) by $\mathcal{E}^{\text{in}}$, which is known. This results in a formula for $\mathcal{E}^{\text{sc}}$ in terms of V:

$$\mathcal{E}^{\text{sc}}(t, \boldsymbol{x}) \approx \mathcal{E}_B(t, \boldsymbol{x}) := \iint g(t - \tau, \boldsymbol{x} - \boldsymbol{z})V(\boldsymbol{z})\mathcal{E}^{\text{in}}(\tau, \boldsymbol{z})\,\mathrm{d}\tau\,\mathrm{d}\boldsymbol{z}. \tag{13}$$

In the frequency domain, the Born approximation is

$$E_B^{\text{sc}}(\omega, \boldsymbol{x}) = -\int \frac{\mathrm{e}^{\mathrm{i}k|\boldsymbol{x}-\boldsymbol{z}|}}{4\pi|\boldsymbol{x} - \boldsymbol{z}|}V(\boldsymbol{z})E^{\text{in}}(\omega, \boldsymbol{z})\,\mathrm{d}\boldsymbol{z}. \tag{14}$$

The Born approximation is very useful, because it makes the imaging problem linear. It is not, however, always a good approximation; see section 5.

3. Inverse synthetic-aperture radar (ISAR)

Radar imaging that uses a fixed antenna and a rotating target is called *Inverse Synthetic-Aperture Radar* (ISAR) [9, 19, 59, 79, 90, 106]. This imaging scheme is typically used for imaging airplanes, spacecraft and ships. In these cases, the target is relatively small and usually isolated.

3.1. The incident field

The incident field $\mathcal{E}^{\text{in}}$ is obtained by solving (2), where s^{in} is taken to be the relevant component of the current density on the source antenna and s^{sc} is zero. For ISAR, we can use a simplified point-like antenna model, for which $s^{\text{in}}(t, \boldsymbol{x}) = p(t)\delta(\boldsymbol{x} - \boldsymbol{x}^0)$, where p is the waveform transmitted by the antenna. Typically p consists of a sequence of time-shifted pulses, so that $p(t) = \sum p_0(t - t_n)$.

In the frequency domain, the corresponding source for (11) is $S^{\text{in}}(\omega, \boldsymbol{x}) = P(\omega)\delta(\boldsymbol{x}-\boldsymbol{x}^0)$, where we write P for the inverse Fourier transform of p:

$$p(t) = \frac{1}{2\pi}\int \mathrm{e}^{-\mathrm{i}\omega t}P(\omega)\,\mathrm{d}\omega. \tag{15}$$

Using (7), we find that the incident field in the frequency domain is

$$\begin{aligned} E^{in}(\omega, \boldsymbol{x}) &= -\int G(\omega, \boldsymbol{x} - \boldsymbol{y})P(\omega)\delta(\boldsymbol{y} - \boldsymbol{x}^0)\,\mathrm{d}\boldsymbol{y} \\ &= -P(\omega)\frac{\mathrm{e}^{\mathrm{i}k|\boldsymbol{x}-\boldsymbol{x}^0|}}{4\pi|\boldsymbol{x} - \boldsymbol{x}^0|}. \end{aligned} \tag{16}$$

3.2. Model for the scattered field

In ISAR, the same antenna is typically used for transmission and reception. Using (16) in (14), we find that the Born-approximated scattered field at the transmitter location $\boldsymbol{x}^0$ is

$$E_B^{sc}(\omega, \boldsymbol{x}^0) = P(\omega) \int \frac{\mathrm{e}^{2\mathrm{i}k|\boldsymbol{x}^0 - \boldsymbol{z}|}}{(4\pi)^2 |\boldsymbol{x}^0 - \boldsymbol{z}|^2} V(\boldsymbol{z})\, \mathrm{d}\boldsymbol{z}. \tag{17}$$

We Fourier transform (17) to write the time-domain field as

$$\begin{aligned} \mathcal{E}_B^{sc}(t, \boldsymbol{x}^0) &= \int\!\!\int \frac{\mathrm{e}^{-\mathrm{i}\omega(t-2|\boldsymbol{x}^0-\boldsymbol{z}|/c)}}{2\pi(4\pi|\boldsymbol{x}^0 - \boldsymbol{z}|)^2} P(\omega) V(\boldsymbol{z})\, \mathrm{d}\omega\, \mathrm{d}\boldsymbol{z} \\ &= \int \frac{p(t - 2|\boldsymbol{x}^0 - \boldsymbol{z}|/c)}{(4\pi|\boldsymbol{x}^0 - \boldsymbol{z}|)^2} V(\boldsymbol{z})\, \mathrm{d}\boldsymbol{z}. \end{aligned} \tag{18}$$

We note the $1/R^2$ geometrical decay (where $R = |\boldsymbol{x}^0 - \boldsymbol{z}|$). When R is large (which it usually is), this results in a received signal that is extremely small; extraction of the signal from noise is typically accomplished by means of a matched filter [27, 35, 69]. Matched filtering results in P of (18) being replaced by $|P|^2$.

3.2.1. The far-field approximation. ISAR also uses the *far-field* or *small-scene* approximation, namely

$$|\boldsymbol{x} - \boldsymbol{y}| = |\boldsymbol{x}| - \hat{\boldsymbol{x}} \cdot \boldsymbol{y} + O\left(\frac{|\boldsymbol{y}|^2}{|\boldsymbol{x}|}\right), \tag{19}$$

where $\hat{\boldsymbol{x}}$ denotes a unit vector in the direction $\boldsymbol{x}$. This approximation is valid for $|\boldsymbol{x}| \gg |\boldsymbol{y}|$.

Using (19) in (4), we obtain the large-$|\boldsymbol{x}|$ expansion of the Green's function [19, 27]

$$G(\omega, \boldsymbol{x} - \boldsymbol{y}) = \frac{\mathrm{e}^{\mathrm{i}k|\boldsymbol{x}-\boldsymbol{y}|}}{4\pi|\boldsymbol{x} - \boldsymbol{y}|} = \frac{\mathrm{e}^{\mathrm{i}k|\boldsymbol{x}|}}{4\pi|\boldsymbol{x}|} \mathrm{e}^{-\mathrm{i}k\hat{\boldsymbol{x}}\cdot\boldsymbol{y}} \left(1 + O\left(\frac{|\boldsymbol{y}|}{|\boldsymbol{x}|}\right)\right)\left(1 + O\left(\frac{k|\boldsymbol{y}|^2}{|\boldsymbol{x}|}\right)\right). \tag{20}$$

Here the first-order term is included in the exponential because k is usually large.

3.2.2. Far-field radar data. In (18), we choose the origin of coordinates to be in or near the target and use the small-scene expansion (20) (with $\boldsymbol{z}$ playing the role of $\boldsymbol{y}$) in the matched-filtered version of (18). This results in the expression for the matched-filtered data:

$$\eta_B(t) = \frac{1}{(4\pi)^2 |\boldsymbol{x}^0|^2} \int \mathrm{e}^{-\mathrm{i}\omega(t-2|\boldsymbol{x}^0|/c + 2\hat{\boldsymbol{x}}^0\cdot\boldsymbol{z}/c)} |P(\omega)|^2 V(\boldsymbol{z})\, \mathrm{d}\omega\, \mathrm{d}\boldsymbol{z}. \tag{21}$$

If we inverse Fourier transform (21), then in the frequency domain we obtain

$$D_B(\omega) = \frac{\mathrm{e}^{2\mathrm{i}k|\boldsymbol{x}^0|}}{(4\pi)^2 |\boldsymbol{x}^0|^2} |P(\omega)|^2 \underbrace{\int \mathrm{e}^{-2\mathrm{i}k\hat{\boldsymbol{x}}^0\cdot\boldsymbol{z}} V(\boldsymbol{z})\, \mathrm{d}\boldsymbol{z}}_{\mathcal{F}[V](2k\hat{\boldsymbol{x}}^0)}. \tag{22}$$

Typical ISAR systems remove the translational motion via tracking and *range alignment* [9, 19], leaving only rotational motion.

3.2.3. Modeling rotating targets. We denote by q the target reflectivity function in the rest frame of the target. Then, as seen by the radar, the reflectivity function is $V(\boldsymbol{x}) = q(\mathcal{O}(\theta_n)\boldsymbol{x})$, where $\mathcal{O}$ is an orthogonal matrix and where $t_n = \theta_n$ denotes the time at the start of the nth pulse of the sequence.

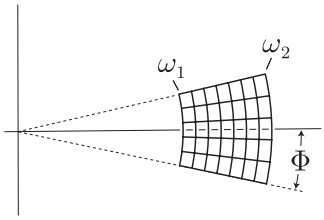

Figure 1. The data-collection manifold for turntable geometry.

For example, if the radar is in the plane perpendicular to the axis of rotation ('turntable geometry'), then the orthogonal matrix $\mathcal{O}$ can be written as

$$\mathcal{O}(\theta) = \begin{pmatrix} \cos\theta & -\sin\theta & 0 \\ \sin\theta & \cos\theta & 0 \\ 0 & 0 & 1 \end{pmatrix} \tag{23}$$

and $V(\boldsymbol{x}) = q(x_1\cos\theta - x_2\sin\theta, x_1\sin\theta + x_2\cos\theta, x_3)$.

3.2.4. Radar data from rotating targets. Using $V(\boldsymbol{x}) = q\,(\mathcal{O}(\theta_n)\boldsymbol{x})$ in (22), we obtain a model for the data from the nth pulse as

$$D_B(\omega,\theta_n) = \frac{\mathrm{e}^{2\mathrm{i}k|\boldsymbol{x}^0|}}{(4\pi)^2|\boldsymbol{x}^0|^2}|P_0(\omega)|^2 \int \mathrm{e}^{-2\mathrm{i}k\widehat{\boldsymbol{x}}^0\cdot\boldsymbol{z}} q(\underbrace{\mathcal{O}(\theta_n)\boldsymbol{z}}_{\boldsymbol{y}})\,\mathrm{d}\boldsymbol{z}. \tag{24}$$

In (24), we make the change of variables $\boldsymbol{y} = \mathcal{O}(\theta_n)\boldsymbol{z}$ and use the fact that the inverse of an orthogonal matrix is its transpose, which means that $\boldsymbol{x}^0\cdot\mathcal{O}^{-1}(\theta_n)\boldsymbol{y} = \mathcal{O}(\theta_n)\boldsymbol{x}^0\cdot\boldsymbol{y}$. We therefore obtain (24) in the form

$$D_B(\omega,\theta_n) = \frac{\mathrm{e}^{2\mathrm{i}k|\boldsymbol{x}^0|}}{(4\pi)^2|\boldsymbol{x}^0|^2}|P_0(\omega)|^2 \underbrace{\int \mathrm{e}^{-2\mathrm{i}k\mathcal{O}(\theta_n)\widehat{\boldsymbol{x}}^0\cdot\boldsymbol{y}} q(\boldsymbol{y})\,\mathrm{d}\boldsymbol{y}}_{\propto\mathcal{F}[q](2k\mathcal{O}(\theta_n)\widehat{\boldsymbol{x}}^0)}. \tag{25}$$

Thus, we see that the frequency-domain data are proportional to the inverse Fourier transform of q, evaluated at an angle determined by the target rotation angle. Consequently, a Fourier transform produces a target image.

The target rotation angle is usually not known. However, if the target is rotating with constant angular velocity, the image produced by the Fourier transform gives rise to a stretched or contracted image, from which the target is usually recognizable [9, 59, 90, 102].

3.3. The data collection manifold

Figure 1 shows an example of a region in Fourier space corresponding to the set $\{2k\mathcal{O}(\theta_n)\widehat{\boldsymbol{x}}^0\}$, where n ranges over the set of pulses, and where $k = \omega/c$ with ω ranging over the angular frequencies received by the radar receiver. The region determined in this manner is called the *data-collection manifold*. The extent of the set of angles is called the *synthetic aperture*, and the extent of the set of frequencies is called the *bandwidth*. Typical synthetic apertures are on the order of a few degrees and typical bandwidths are $2\pi \times 500 \times 10^6$ rad s^{-1}.

ISAR resolution [63, 90] depends on the size and extent of the data collection manifold.

Examples of ISAR images are shown in figures 2 and 3.

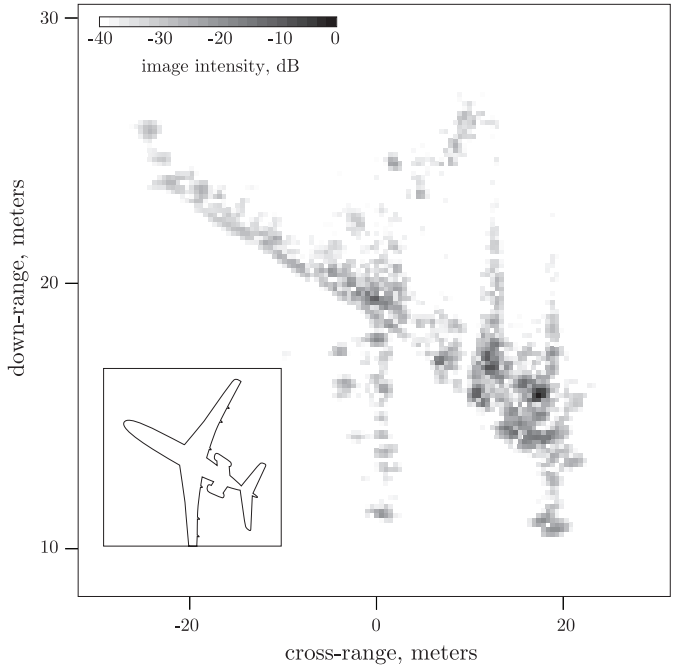

Figure 2. An ISAR image of a Boeing 727 from a $2\Phi \approx 5^\circ$ aperture [95].

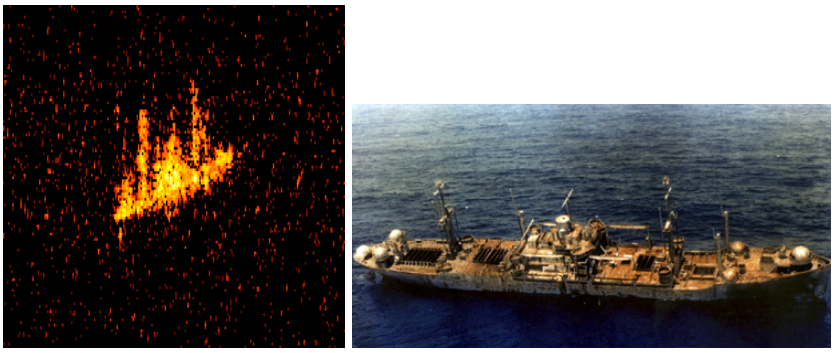

Figure 3. On the left is an ISAR image of a ship; on the right is an optical image of the same ship. (Courtesy Naval Research Laboratory)

3.4. ISAR *in the time domain*

We Fourier transform (25) into the time domain, obtaining

$$\eta_B(t,\theta_n) \propto \int\int \mathrm{e}^{-\mathrm{i}\omega(t-2|\boldsymbol{x}^0|/c+2\mathcal{O}(\theta_n)\widehat{\boldsymbol{x}}^0\cdot\boldsymbol{y}/c)}|P_0(\omega)|^2\,\mathrm{d}\omega q(\boldsymbol{y})\,\mathrm{d}\boldsymbol{y}. \tag{26}$$

If we evaluate η_B at a shifted time, we obtain the simpler expression

$$\eta_B\left(t+\frac{2|\boldsymbol{x}^0|}{c},\theta_n\right) = \int\int \mathrm{e}^{-\mathrm{i}\omega(t+2\mathcal{O}(\theta_n)\widehat{\boldsymbol{x}}^0\cdot\boldsymbol{y}/c)}|P_0(\omega)|^2\,\mathrm{d}\omega q(\boldsymbol{y})\,\mathrm{d}\boldsymbol{y}. \tag{27}$$

We temporarily write $\tau = -2\mathcal{O}(\theta_n)\boldsymbol{x}^0 \cdot \boldsymbol{y}/c$ and write the ω integral on the right-hand side of (27) as

$$\int \mathrm{e}^{-\mathrm{i}\omega(t-\tau)}|P_0(\omega)|^2\,\mathrm{d}\omega = \int \delta(s-\tau)\beta(t-s)\,\mathrm{d}s, \tag{28}$$

where

$$\beta(t-s) = \int \mathrm{e}^{-\mathrm{i}\omega(t-s)}|P_0(\omega)|^2\,\mathrm{d}\omega.$$

With (28), we can write η_B as

$$\eta_B\left(t + \frac{2|\boldsymbol{x}^0|}{c}, \theta_n\right) = \int \beta(t-s)\int \delta\left(s + \frac{2\mathcal{O}(\theta_n)\widehat{\boldsymbol{x}^0}}{c}\cdot\boldsymbol{y}\right) q(\boldsymbol{y})\,\mathrm{d}\boldsymbol{y}\,\mathrm{d}s$$
$$= \beta * \mathcal{R}[q]\left(\frac{-2\mathcal{O}(\theta_n)\widehat{\boldsymbol{x}^0}}{c}\right),$$

where

$$\mathcal{R}[q](s, \widehat{\boldsymbol{\mu}}) = \int \delta(s - \widehat{\boldsymbol{\mu}}\cdot\boldsymbol{y})q(\boldsymbol{y})\,\mathrm{d}\boldsymbol{y} \tag{29}$$

is the *Radon transform* [62, 64]. Here $\widehat{\boldsymbol{\mu}}$ denotes a unit vector. In other words, the Radon transform of q is defined as the integral of q over the plane $s = \hat{\boldsymbol{\mu}}\cdot\boldsymbol{y}$.

ISAR systems typically use a high-range-resolution (large bandwidth) waveform, so that $\beta \approx \delta$. Thus ISAR imaging from time-domain data becomes a problem of inverting the Radon transform.

4. Synthetic-aperture radar

Synthetic-aperture radar (SAR) [16, 28, 29, 40, 49, 82] involves a moving antenna, and usually the antenna is pointed toward the Earth. For an antenna viewing the Earth, we need to include a model for the antenna beam pattern, which describes the directivity of the antenna. For highly directive antennas, we often simply refer to the antenna 'footprint', which is the illuminated area on the ground.

If we assume that the receiving antenna is at the same location as the transmitting antenna, then we find that the scalar Born model for the received signal is

$$S_B(\omega) = \int \mathrm{e}^{2\mathrm{i}k|\boldsymbol{x}^0-\boldsymbol{y}|}A(\omega, \boldsymbol{x}^0, \boldsymbol{y})V(\boldsymbol{y})\,\mathrm{d}\boldsymbol{y}, \tag{30}$$

where A incorporates the geometrical spreading factors $|\boldsymbol{x}^0 - \boldsymbol{y}|^{-2}$, transmitted waveform and antenna beam pattern. More details can be found in [19].

For a pulsed system, we assume that pulses are transmitted at times t_n, and we denote the antenna position at time t_n by $\boldsymbol{\gamma}_n$. Because the timescale on which the antenna moves is much slower than the timescale on which the electromagnetic waves propagate, we separate the time scales into a *slow time*, which corresponds to n of t_n, and a *fast time* t.

In (30) we replace the antenna position $\boldsymbol{x}^0$ by $\boldsymbol{\gamma}_n$:

$$D(\omega, n) = F[V](\omega, s) := \int \mathrm{e}^{2\mathrm{i}k|\boldsymbol{\gamma}_n-\boldsymbol{y}|}A(\omega, n, \boldsymbol{y})V(\boldsymbol{y})\,\mathrm{d}\boldsymbol{y}, \tag{31}$$

where with a slight abuse of notation we have replaced $\boldsymbol{x}^0$ in the argument of A by n. This notation also allows for the possibility that the waveform and antenna beam pattern could be different at different points along the flight path. The time-domain version of (31) is

$$d(t, n) = \int \mathrm{e}^{-\,\mathrm{i}\,\omega[t-2|\boldsymbol{\gamma}_n-\boldsymbol{y}|/c]}A(\omega, n, \boldsymbol{y})V(\boldsymbol{y})\,\mathrm{d}\boldsymbol{y}. \tag{32}$$

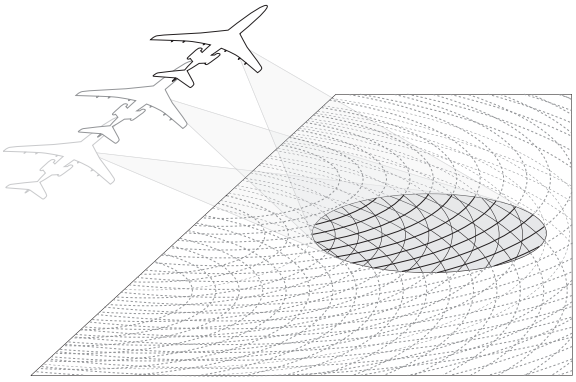

Figure 4. In spotlight SAR the radar is trained on a particular location as the radar moves. In this figure, the equi-range circles (dotted lines) are formed from the intersection of the radiated spherical wavefront and the surface of a (flat) earth.

The goal of SAR is to determine V from the data d.

As in the case of ISAR, assuming that $\boldsymbol{\gamma}$ and A are known, the data depend on two variables, so we expect to form a two-dimensional image. For typical radar frequencies, most of the scattering takes place in a thin layer at the surface. We therefore assume that the ground reflectivity function V is supported on a known surface. For simplicity we take this surface to be a flat plane, so that $V(\boldsymbol{x}) = V(\mathbf{x})\delta(x_3)$, where $\mathbf{x} = (x_1, x_2)$.

SAR imaging comes in two basic varieties: *spotlight* SAR [16, 49] and *stripmap* SAR [28, 29, 40, 82].

4.1. Spotlight SAR

Spotlight SAR is illustrated in figure 4. Here the moving radar system stares at a specific location (usually on the ground) so that at each point in the flight path the same target is illuminated from a different direction. When the ground is assumed to be a horizontal plane, the iso-range curves are large circles whose centers are directly below the antenna at $\boldsymbol{\gamma}_n$. If the radar antenna is highly directional and the antenna footprint is sufficiently far away, then the circular arcs within the footprint can be approximated as lines. Consequently, the imaging method is mathematically the same as that used in ISAR.

In particular, we put the origin of coordinates in the footprint, use the far-field expansion, and obtain for the matched-filtered frequency-domain data

$$D(\omega, n) = \mathrm{e}^{2\mathrm{i}k|\boldsymbol{\gamma}_n|} \int \mathrm{e}^{2\mathrm{i}k\widehat{\boldsymbol{\gamma}}_n \cdot \boldsymbol{y}} V(\boldsymbol{y}) A(\omega, n, \boldsymbol{y})\, \mathrm{d}\boldsymbol{y}. \tag{33}$$

We approximate A within the footprint as a product $A = A_1(\omega, n)A_2(\boldsymbol{y})$. The function A_1 can be taken outside the integral; the function A_2 can be divided out after inverse Fourier transforming.

As in the ISAR case, the time-domain formulation of spotlight SAR leads to a problem of inverting the Radon transform.

4.2. Stripmap SAR

Just as the time-domain formulations of ISAR and spotlight SAR reduce to inversion of the Radon transform, which is a tomographic inversion of an object from its integrals over lines

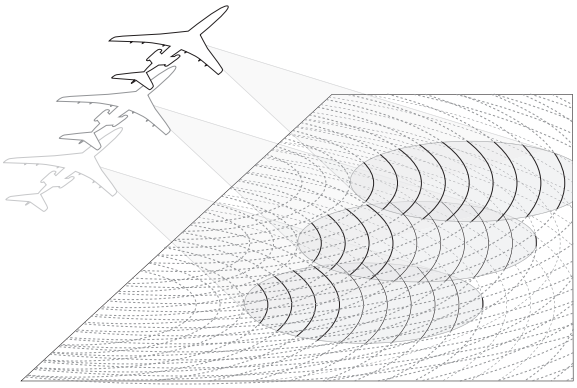

Figure 5. Stripmap SAR acquires data without staring. The radar typically has fixed orientation with respect to the flight direction and the data are acquired as the beam footprint sweeps over the ground.

or planes, stripmap SAR also reduces to a tomographic inversion of an object from its integrals over circles or spheres (see figure 5). For a derivation of the mathematical model for stripmap SAR and a discussion of associated issues and open problems, we refer the reader to [19]. Image formation algorithms can be found in [19, 28, 29, 40, 82].

5. Open problems

In the decades since the invention of synthetic-aperture radar imaging, there has been much progress, but many open problems still remain. And most of these open problems are mathematical in nature.

5.1. Design of incident fields for particular purposes

(i) How can we find waveforms that are optimal for identifying certain targets (see [52, 42]). What polarization is best for this [44]? The best waveforms would not only enhance scattering from targets of interest, but would also tend to reject clutter (targets that are not of interest) and noise (see [31, 81, 100, 112, 113]).

(ii) Given a desired power spectrum, find a *constant-amplitude* causal waveform that best approximates the desired one [74]. (Here 'power spectrum' means the squared magnitude of the Fourier transform.) The constraint of constant amplitude is important for amplifier efficiency.

(iii) How can we best exploit the emerging technology of digital waveform generation for use in imaging? It is now possible to build array antennas in which each element is connected to a different signal generator, so that each element can be fed a different waveform. What can be done with such an *agile antenna*? What waveforms should be used for which purposes? How should the different waveforms be scheduled to adapt to a changing scene? These questions apply both in the case when antenna elements are close to each other and when they are far apart. More information about antennas can be found in [19, 89].

5.2. Problems related to synthetic-aperture imaging

(i) How can we form images without using the Born approximation? The Born approximation leaves out many physical effects, including not only multiple scattering and creeping waves, but also shadowing, obscuration and polarization changes. But without the Born approximation (or the Kirchhoff approximation, which is similar), the imaging problem is nonlinear. In particular, how can we form images in the presence of multiple scattering? (See [10, 20, 43, 67, 105].) Can multiple scattering be exploited to improve resolution? (See [56].)

(ii) We need to develop scattering models that include as much of the physics as possible, but that are still simple enough for use in the inverse problem. An example of a simple model that includes relevant physics is [77].

(iii) Both SAR and ISAR are based on known relative motion between target and sensor, but often this motion is not known well enough to form well-focused images. Better methods for finding the relative motion between target and sensor are also needed [10, 88]. Better algorithms are needed for determining the antenna position from the radar data itself. Such methods include *autofocus* algorithms [49, 57], some of which use a criterion such as image contrast to focus the image.

(iv) When the target motion is complex (pitching, rolling and yawing), it may be possible to form a three-dimensional image; fast, accurate methods for doing this are needed [88]. How can we simultaneously track [78] moving objects and form 3D images of them?

(v) How can we mitigate the artifacts associated with targets that move during data collection [75]? Moving targets cause Doppler shifts, and also present different aspects to the radar [18]. An approach for exploiting unknown motion is given in [88].

(vi) Synthetic-aperture imaging techniques need to be more fully developed for the case of a small number of transmitters and receivers [18, 33, 101, 107, 108, 115], which could be positioned far from each other. In this *multistatic* situation, synthetic apertures and real apertures are combined. For example, methods need to be developed for registering the various disparate signals to a common time origin. Methods need to be developed for handing sparse data [24].

(vii) We would like to develop fast imaging [11, 33, 111] and target-classification/identification algorithms. The latter deal with the problem of identifying an unknown target from a SAR or ISAR image. For example, from radar images of a scene, can we identify not only the vehicles, but also the vehicle type [22] and even individual vehicles? This problem may be closely related to computer vision. Target classification and identification algorithms ideally should run in real time. (See figures 6 and 7.)

(viii) Theoretical bounds are needed for the target-classification/identification problem [51].

(ix) How can we incorporate prior knowledge about the scene to improve resolution? We would like to go beyond simple aperture/bandwidth-defined resolution [63, 90]. One approach that has been suggested is to apply compressive sensing ideas [4, 22, 61] to SAR.

(x) How can we fully exploit the polarization information [14, 21, 26, 76, 99] in the scattered field? This problem is closely connected to the issue of multiple scattering: we do not have a linear model that predicts any change in the polarization of the backscattered electric field. Consequently our linear imaging methods cannot provide information about how scatterers change the polarization of the interrogating field. A paper that may be useful here is [94].

(xi) How can we exploit the information in the radar shadow? In many cases, it is easier to identify an object from its shadow than from its direct-scattering image. (See figure 8.) A backprojection method for reconstructing an object's three-dimensional shape from its

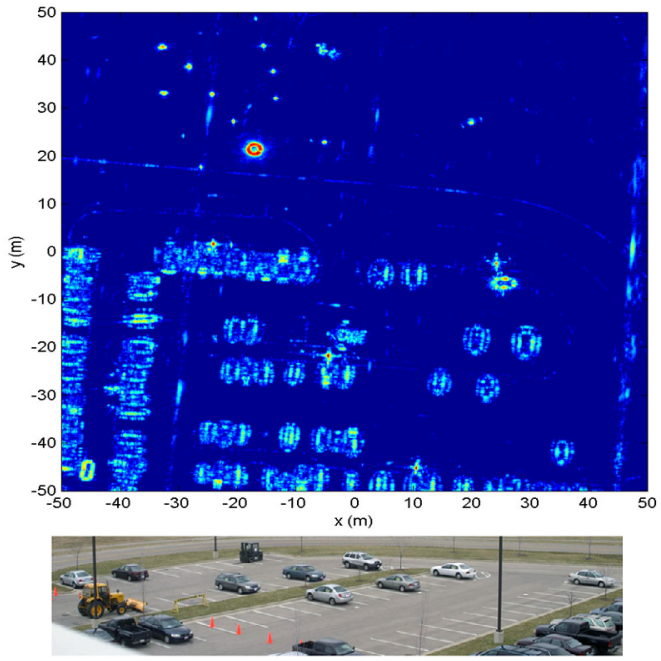

Figure 6. A radar image from a circular flight path, together with an optical image of the same scene. The bright ring in the top half of the radar image is a 'top-hat' calibration target used to focus the image. (Courtesy U.S. Air Force Sensors Directorate)

shadows obtained at different viewing angles is proposed in [32]. What determines the resolution of this reconstruction?

(xii) Typical radar frequencies are scattered by forest canopies and foliage. Lower frequencies penetrate better, but result in lower resolution images. How can we extract the most information from foliage-penetrating (FOPEN) SAR ? Moreover, in forested areas, multiple scattering may be important, whereas the known methods for forming images neglect multiple scattering. We would like to be able to obtain the bare-earth topography and identify objects beneath foliage. We would also like to assess the forest itself [3, 23]; probably the forest should be modeled as a random medium [50, 83, 94, 97]. The forestry industry would like information about tree health and trunk volume, and climate modelers would like to know the forest biomass [34, 92].

(xiii) How can we extract the most information from over-the-horizon (OTH) radar [105], in which electromagnetic waves are bounced off the ionosphere? The ionosphere is a complicated and rapidly changing medium that strongly affects low-frequency radio waves. It is also dispersive, meaning that different frequencies propagate with different speeds.

(xiv) How can we best use ground-penetrating radar (GPR or GPEN) [5, 15, 76] to obtain information about the ground and structures within it? Soil is a more complicated medium than air, which implies that the corresponding imaging problem is more difficult. In addition, because the antenna is so close to the Earth, the approximations made in section 3.2.1 do not apply, and in fact the antenna properties change depending on what is in the soil. GPR is of interest in many areas. Global climate modelers would like to

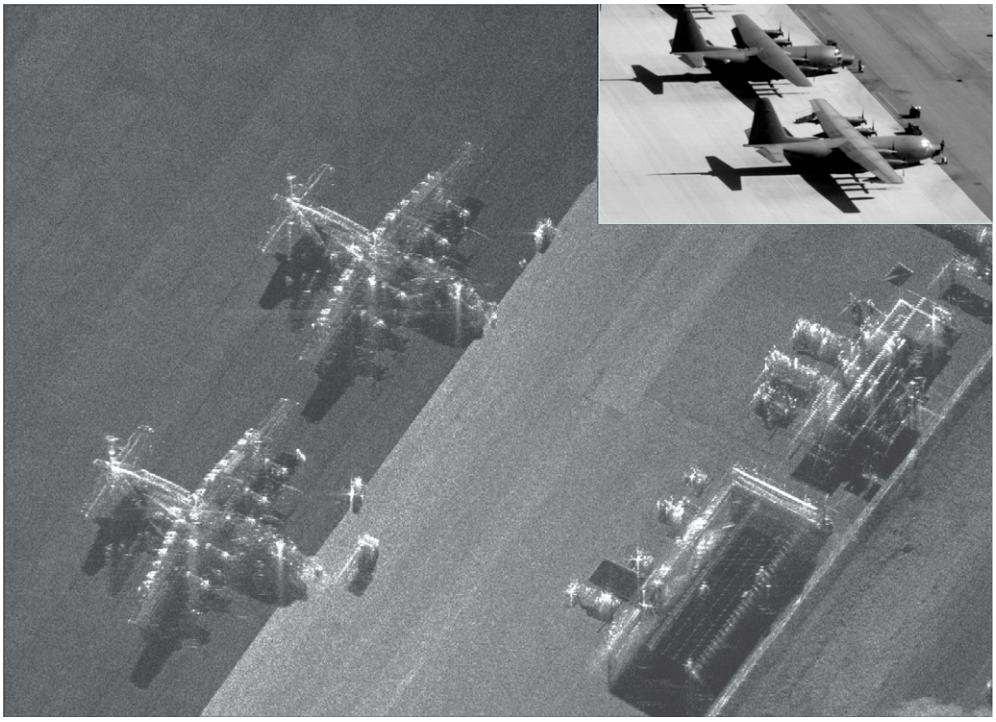

Figure 7. A 4 inch resolution SAR image from Sandia National Laboratories. Note that only certain parts of the airplanes reflect radar energy. The inset is an optical image of the airplanes. (Courtesy Sandia National Laboratories)

Figure 8. A 4 inch resolution image from Sandia National Laboratories. Note the shadows of the historical airplane, helicopter and trees. (Courtesy Sandia National Laboratories)

access ice thickness and depth profiles. Civil engineers use GPR to assess the condition of roads and bridges, and to identify buried utilities. Archaeologists use GPR to find sites of archaeological interest. GPR systems are being developed to identify land mines [5], unexploded ordinance (UXO) and underground bunkers.

(xv) How can we do radar imaging through walls [1] and rubble [2]? This can be important for finding victims in disaster areas. We would like to use radar to obtain the building layout and determine where people are located. In many cases, details of the construction of the wall may not be known. How does furniture such as metal desks and file cabinets affect the scattering? Can we detect breathing and heartbeat by exploiting the Doppler shift [21] in the radar signals, even if we cannot form an image?

(xvi) Can we use radar to identify individuals by their gestures or gait? Time–frequency analysis of radar signals gives rise to *micro-Doppler* time–frequency images [21], in which the motion of arms and legs can be identified.

(xvii) How can we best do radar imaging of urban areas? It is difficult to form SAR images of urban areas, because in cities the waves undergo complicated multipath scattering. Areas behind buildings lie in the radar shadows, and images of tall buildings can obscure other features of interest. In addition, urban areas tend to be sources of electromagnetic radiation that can interfere with the radiation used for imaging. One approach that is being explored is to use a *persistent* or *staring* radar system [37] that would fly in circles [84] around a city of interest. Thus, the radar would eventually illuminate most of the areas that would be shadowed when viewed from a single direction. However, this approach has the added difficulty that that same object will look different when viewed from different directions. How can the data from a staring radar system be used to obtain the maximum amount of information about the (potentially changing) scene?

(xviii) How can we use radar for medical imaging? This area is sometimes called microwave tomography [8, 80]. It should be possible to use microwaves to form images of the interior of the human body. For this, the far-field approximation is probably inappropriate. We may want to use multiple antennas.

(xix) It is now possible to build radar systems with multiple transmitters and receivers located at different positions. These are often called *multiple-input, multiple-output* (MIMO) radar systems [58]. What can be done with such a system? Particularly, if a small number of transmitters and receivers are available, where should they be positioned [18, 98, 110]? How often should they be active? How can images best be formed when sparse, random networks of antennas are used? Is it possible to exploit radiation from radio and TV stations to form images [46, 114, 115]?

(xx) If sensors are flown on unoccupied aerial vehicles, where should these UAVs fly? The notion of swarms of UAVs [13] gives rise not only to challenging problems in control theory, but also challenging imaging problems.

(xxi) In many specific applications, we need to learn how to extract useful information from radar images and radar data. For example, in images of the arctic regions, can we determine ice thickness [73]? For medical microwave tomography, can we determine tissue health from knowledge of the tissue electromagnetic parameters? (See also (xii) above.) To assess crop health, ice thickness and tissue health, how can we combine information from different frequency bands, and how can we combine radar images with those from different sensors such as optical or acoustic ones? Some of these problems will require an understanding of scattering physics.

(xxii) Many of these problems motivate a variety of more theoretical open problems, such as the question of whether backscattered data uniquely determine a penetrable object or a non-convex surface [86, 102]. There is a close connection between radar imaging and

the theory of Fourier integral operators [66]. How can this theory be extended to the case of dispersive media and to nonlinear operators? How can we develop a theory of the information content [54, 71] of an imaging system?

Radar imaging is a mathematically rich field that is ready for more mathematical attention!

Acknowledgments

The authors would like to thank the Naval Postgraduate School and the Air Force Office of Scientific Research[3], which supported this work under agreement no. FA9550-09-1-0013.

References

[1] Ahmad F and Amin M G 2006 Noncoherent approach to through-the-wall radar localization *IEEE Trans. Aerospace Electron. Syst.* **42** 1405–19
[2] Arai I 2001 Survivor search radar system for persons trapped under earthquakerubble *Asia-Pacific Microwave Conf.* vol 2, pp 663–8
[3] Askne J I H, Dammert P B G, Ulander L M H and Smith G 1997 C-band repeat-pass interferometric SAR observations of the forest *IEEE Trans. Geosci. Remote Sensing* **35** 25–35
[4] Baraniuk R and Steeghs P 2007 Compressive radar imaging *IEEE Radar Conference, Waltham,* MA
[5] Baum C E 1999 *Detection and Identification of Visually Obscured Targets* (London: Taylor and Francis Inc.)
[6] Bowen E G 1987 *Radar Days* (Bristol: Hilgar)
[7] Bleistein N, Cohen J K and Stockwell J W 2000 *The Mathematics of Multidimensional Seismic Inversion* (New York: Springer)
[8] Bond E J, Li X, Hagness S C and Van Veen B D 2003 Microwave imaging via space-time beamforming for early detection of breast cancer *IEEE Trans. Antennas Propag.* **51** 1690–705
[9] Borden B 1999 *Radar Imaging of Airborne Targets* (Bristol: Institute of Physics)
[10] Borden B 2002 Mathematical problems in radar inverse scattering *Inverse Problems* **18** R1–R28
[11] Brandfass M and Chew W C 2000 Microwave imaging as applied to remote sensing making use of a multilevel fast multipole algorithm *Algorithms for Synthetic Aperture Radar Imagery VII Proc. SPIE 4053* ed E G Zelnio (Orlando, FL) 52–63
[12] Buderi R 1996 *The Invention that Changed the World* (New York: Simon and Schuster)
[13] Bethke B, Valenti M, How J P and Vian J 2007 Cooperative vision based estimation and tracking using multiple UAVs *Conf. on Cooperative Control and Optimization* (Gainesville, FL)
[14] Boerner W-M and Yamaguchi Y 1990 A state-of-the-art review in radar polarimetry and its applications in remote sensing *IEEE Aerospace Electron. Syst. Mag.* **5** 3–6
[15] Carin L, Geng N, McClure M, Sichina J and Nguyen L 1999 Ultra-wide-band synthetic-aperture radar for mine-field detection *IEEE Antennas Propag. Mag.* **41** 18–33
[16] Carrara W C, Goodman R G and Majewski R M 1995 *Spotlight Synthetic Aperture Radar: Signal Processing Algorithms* (Boston: Artech House)
[17] Cheney M 2001 A mathematical tutorial on Synthetic Aperture Radar *SIAM Rev.* **43** 301–12
[18] Cheney M and Borden B 2008 Imaging moving targets from scattered waves *Inverse Problems* **24** 035005
[19] Cheney M and Borden B 2009 *Fundamentals of Radar Imaging* (Philadelphia: SIAM)
[20] Cheney M and Bonneau R J 2004 Imaging that exploits multipath scattering from point scatterers *Inverse Problems* **20** 1691–711
[21] Chen V C and Ling H 2002 *Time–Frequency Transforms for Radar Imaging and Signal Analysis* (Boston: Artech House)
[22] Çetin M, Karl W C and Castañon D A 2002 Analysis of the impact of feature-enhanced SAR imaging on ATR performance *Algorithms for SAR Imagery IX Proc. SPIE* vol 4727
[23] Chen J, Simonett D S and Sun G 1988 Computer-aided interpretation of forest radar images *Pattern Recognit.* **2** 1245–9

[3] Consequently, the US Government is authorized to reproduce and distribute reprints for Governmental purposes notwithstanding any copyright notation thereon. The views and conclusions contained herein are those of the authors and should not be interpreted as necessarily representing the official policies or endorsements, either expressed or implied, of the Air Force Research Laboratory or the US Government.

[24] Chew W C and Song J M 2000 Fast Fourier transform of sparse spatial data to sparse Fourier data *IEEE Antenna Propag. Int. Symp.* **4** 2324–7

[25] Cloude S R 2006 Polarization coherence tomography *Radio Sci.* **41** RS4017 doi:10.1029/2005RS003436

[26] Cloude S R and Papathanassiou K P 1998 Polarimetric SAR interferometry *IEEE Trans. Geosci. Remote Sensing* **36** 1551–65

[27] Cook C E and Bernfeld M 1967 *Radar Signals* (New York: Academic)

[28] Cumming I G and Wong F H 2005 *Digital Processing of Synthetic Aperture Radar Data: Algorithms and Implementation* (Boston, MA: Artech House)

[29] Curlander J C and McDonough R N 1991 *Synthetic Aperture Radar* (New York: Wiley)

[30] Cutrona L J 1990 Synthetic aperture radar *Radar Handbook* 2nd edn, ed M Skolnik (New York: McGraw-Hill)

[31] DeLong D and Hofstetter E 1967 On the design of optimum radar waveforms for clutter rejection *IEEE Trans. Inf. Theory* **13** 454– 463

[32] Dickey F M and Doerry A W 2008 Recovering shape from shadows in synthetic aperture radar imagery *Radar Sensor Technology XII Proc. SPIE* vol 6947 ed Kenneth I Ranney and Armin W Doerry 694707

[33] Ding Y and Munson D C Jr 2002 A fast back-projection algorithm for bistatic SAR imaging *Proc. IEEE Int. Conf. on Image Processing* (Rochester, NY, 22–25 Sept)

[34] Dobson M C *et al* 1995 Estimation of forest biophysical characteristics in Northern Michigan with SIR-c/X-SAR *IEEE Trans. Geosci. Remote Sensing* **33** 877–95

[35] Edde B 1993 *Radar: Principles, Technology, Applications* (Englewood Cliffs, NJ: Prentice-Hall)

[36] Elachi C 1987 *Spaceborne Radar Remote Sensing: Applications and Techniques* (New York: IEEE)

[37] Ertin E, Austin C D, Sharma S, Moses R L and Potter L C 2007 GOTCHA experience report: three-dimensional SAR imaging with complete circular apertures *Proc. SPIE* **6568** 656802

[38] Fisher D E 1988 *A Race on the Edge of Time: Radar—the Decisive Weapon of World War II* (New York: McGraw-Hill)

[39] Fienup J R 2001 Detecting moving targets in SAR imagery by focusing *IEEE Trans. Aero. Electr. Syst.* **37** 794–809

[40] Franceschetti G and Lanari R 1999 *Synthetic Aperture Radar Processing* (New York: CRC Press)

[41] Friedlander F G 1982 *Introduction to the Theory of Distributions* (New York: Cambridge University Press)

[42] Garren D A, Odom A C, Osborn M K, Goldstein J S, Pillai S U and Guerci J R 2002 Full-polarization matched-illumination for target detection and identification *IEEE Trans. Aerospace Electron. Syst.* **38** 824– 837

[43] Garnier J and Sølna K 2008 Coherent interferometric imaging for synthetic aperture radar in the presence of noise *Inverse Problems* **24** 055001

[44] Giuli D 1986 Polarization diversity in radars *Proc. the IEEE* **74** 245–69

[45] Greengard L and Lee J-Y 2004 Accelerating the nonuniform fast Fourier transform *SIAM Rev.* **46** 443–54

[46] Griffiths H D and Baker C J 2005 Measurement and analysis of ambiguity functions of passive radar transmissions *IEEE Int. Radar Conf.* 321–5

[47] Grigis A and Sjöstrand J 1994 *Microlocal Analysis for Differential Operators: An Introduction* (*London Mathematical Society Lecture Note Series* vol 196) (Cambridge: Cambridge University Press)

[48] Jackson J D 1962 *Classical Electrodynamics* 2nd edn (New York: Wiley)

[49] Jakowatz C V, Wahl D E, Eichel P H, Ghiglia D C and Thompson P A 1996 *Spotlight-Mode Synthetic Aperture Radar: A Signal Processing Approach* (Boston: Kluwer)

[50] Ishimaru A 1997 *Wave Propagation and Scattering in Random Media* (New York: IEEE)

[51] Jain A, Moulin P, Miller M I and Ramchandran K 2000 Information-Theoretic bounds on target recognition performance *Automatic Target Recognition X, Proc. SPIE* vol 4050, ed F A Sadjadi (Orlando, FL) pp 347–358

[52] Kennaugh E M 1981 The K-pulse concept *IEEE Trans. Antennas Propag.* **29** 327–31

[53] Klemm R 2002 *Principles of Space-Time Adaptive Processing* (London: Institution of Electrical Engineers)

[54] Klug A and Crowther R A 1972 Three-dimensional image reconstruction from the viewpoint of information theory *Nature* **238** 435–40 doi:10.1038/238435a0

[55] Langenberg K J, Brandfass M, Mayer K, Kreutter T, Brüll A, Felinger P and Huo D 1993 Principles of microwave imaging and inverse scattering *EARSeL Adv. Remote Sens.* **2** 163–86

[56] Lerosey G, de Rosny J, Tourin A and Fink M 2007 Focusing beyond the diffraction limit with far-field time reversal *Science* **315** 1120–2

[57] Lee-Elkin F 2008 Autofocus for 3D imaging *Proc. SPIE* **6970** 69700O

[58] J Li and Stoica P 2008 *MIMO Radar Signal Processing* (New York: Wiley)

[59] Mensa D L 1981 *High Resolution Radar Imaging* (Dedham, MA: Artech House)

[60] Bárcenas J H M 2008 Synthetic-aperture radar imaging and waveform design for dispersive media *PhD Thesis* Rensselaer Polytechnic Institute, Troy, NY

[61] Moses R, Çetin M and Potter L 2004 Wide angle SAR imaging *SPIE Algorithms for Synthetic Aperture Radar Imagery XI* (Orlando, FL)
[62] Natterer F 2001 *The Mathematics of Computerized Tomography* (Philadelphia: SIAM)
[63] Natterer F, Cheney M and Borden B 2003 Resolution for radar and X-ray tomography *Inverse Problems* **19** S55–64
[64] Natterer F and Wübbeling F 2001 *Mathematical Methods in Imaging Reconstruction* (Philadelphia: SIAM)
[65] Newton R G 2002 *Scattering Theory of Waves and Particles* (Mineola, NY: Dover)
[66] Nolan C J and Cheney M 2003 Synthetic aperture inversion for arbitrary flight paths and non-flat topography *IEEE Trans. on Image Processing* **12** 1035–43
[67] Nolan C J, Cheney M, Dowling T and Gaburro R 2006 Enhanced angular resolution from multiply scattered waves *Inverse Problems* **22** 1817–34
[68] Nolan C J and Symes W W 1997 Global solution of a linearized inverse problem for the acoustic wave equation *Comm. P.D.E.* **22** 919–52
[69] North D O 1943 Analysis of the factors which determine signal/noise discrimination in radar *Report PPR 6C Reproduction* (Princeton, NJ: RCA Laboratories classified)
North D O 1963 An analysis of the factors which determine signal/noise discrimination in pulsed-carrier systems *Proc. IEEE* **51** 1016–27
[70] Oppenheim A V and Shafer R W 1975 *Digital Signal Processing* (Englewood Cliffs, NJ: Prentice-Hall)
[71] O'Sullivan J A, Blahut R E and Snyder D L 1998 Information-theoretic image formation *IEEE Trans. Inf. Theory* **44** 2094–123
[72] Oughstun K E and Sherman G C 1997 *Electromagnetic Pulse Propagation in Causal Dielectrics* (New York: Springer)
[73] Paden J, Mozaffar S, Dunson D, Allen C, Gogineni S and Akins T 2004 Multiband multistatic synthetic aperture radar for measuring ice sheet basal conditions *Proc. IGARSS'04* (Anchorage, AK)
[74] Patton L K and Rigling B D 2008 Modulus constraints in adaptive radar waveform design *Proc. IEEE Radar Conf.* pp 1–6
[75] Perry R P, DiPietro R C and Fante R L 1999 SAR imaging of moving targets *IEEE Trans. Aerospace Electron. Syst.* **35** 188–200
[76] Pike R and Sabatier P 2002 *Scattering: Scattering and Inverse Scattering in Pure and Applied Science* (New York: Academic)
[77] Potter L C and Moses R L 1997 Attributed scattering centers for SAR ATR *IEEE Trans. Image Process.* **6** 79–91
[78] Ramachandra K V 2000 *Kalman Filtering Techniques for Radar Tracking* (Boca Raton, FL: CRC Press)
[79] Rihaczek A W 1969 *Principles of High-Resolution Radar* (New York: McGraw-Hill)
[80] Semenov S Y 1999 Three dimensional microwave tomography. Experimental prototype of the system and vector Born reconstruction method *IEEE Trans. BME* **46** 937–46
[81] Sira S P, Cochran D, Papandreou-Suppappola A, Morrell D, Moran W, Howard S D and Calderbank R 2007 Adaptive waveform design for improved detection of low-RCS targets in heavy sea clutter *IEEE J. Sel. Topics in Signal Processing* **1** 56–66
[82] Skolnik M 1980 *Introduction to Radar Systems* (New York: McGraw-Hill)
[83] Sobczyk K 1985 *Stochastic Wave Propagation* (New York: Elsevier)
[84] Soumekh M 1999 *Synthetic Aperture Radar Signal Processing with MATLAB Algorithms* (New York: Wiley)
[85] Stakgold I 1997 *Green's Functions and Boundary Value Problems* 2nd edn (New York: Wiley-Interscience)
[86] Stefanov P and Uhlmann G 1997 Inverse backscattering for the acoustic equation *SIAM J. Math. Anal.* **28** 1191–204
[87] Stimson G W 1998 *Introduction to Airborne Radar* (Mendham, NJ: SciTech)
[88] Stuff M A, Sanchez P and Biancala M 2003 Extraction of three-dimensional motion and geometric invariants *Multidimens. Syst. Signal Process.* **14** 161–81
[89] Stutzman W L and Thiele G A 1998 *Antenna Theory and Design* (New York: Wiley)
[90] Sullivan R J 2004 *Radar Foundations for Imaging and Advanced Concepts* (Raleigh, NC: SciTech)
[91] Swords S S 1986 *Technical History of the Beginnings of Radar* (London: Peregrinus)
[92] Le Toan T, Beaudoin A, Riom J and Guyon D 1992 Relating forest biomass to SAR data *IEEE Trans. Geosci. Remote Sensing* **30** 403–11
[93] Treves F 1975 *Basic Linear Partial Differential Equations* (New York: Academic)
[94] Treuhaft R N and Siqueira P R 2000 Vertical structure of vegetated land surfaces from interferometric and polarimetric radar *Radio Science* **35** 141–77
[95] Trischman J A, Jones S, Bloomfield R, Nelson E and Dinger R 1994 An X-band linear frequency modulated radar for dynamic aircraft measurement *AMTA Proc.* (New York: AMTA) p 431

[96] Tsynkov S 2008 On *sar* imaging through the earth ionosphere *SIAM J. Imaging Sci.*
[97] Tsang L, Kong J A and Shin R T 1985 *Theory of Microwave Remote Sensing* (New York: Wiley)
[98] Tsao T, Slamani M, Varshney P, Weiner D, Schwarzlander H and Borek S 1997 Ambiguity function for bistatic radar *IEEE Trans. Aerospace Electron. Syst.* **AES-33** 1041–51
[99] Ulaby F T and Elachi C 1990 *Radar Polarimetry for Geoscience Applications* (Norwood, MA: Artech House)
[100] Varslot T, Yarman C E, Cheney M and Yazici B 2007 A variational approach to waveform design for synthetic-aperture imaging *Inverse Problems Imaging* **1** 577–92
[101] Varslot T, Yazici B and Cheney M 2008 Wideband pulse-echo imaging with distributed apertures in multi-path environments *Inverse Problems* **24** 045013
[102] Walsh T E 1978 Military radar systems: history, current position, and future forecast *Microw. J.* **21** 87, 88, 91–95
[103] Wang J-N 1998 Inverse backscattering problem for Maxwell's equations *Math. Methods Appl. Sci.* **21** 1441–65
[104] Wang G, Xia X-G, Root B T, Chen V C, Zhang Y and Amin M 2003 Manoeuvring target detection in over-the-horizon radar using adaptive clutter rejection and adaptive chirplet transform *IEE Proc. on Radar, Sonar and Navigation* **150** 292–8
[105] Weglein A B, Araùjo F V, Carvalho P M, Stolt R H, Matson K H, Coates R T, Corrigan D, Foster D J, Shaw S A and Zhang H 2003 Inverse scattering series and seismic exploration *Inverse Problems* **19** R27–83
[106] Wehner D 1995 *High-Resolution Radar* 2nd edn (Raleigh, NC: Scitech)
[107] Willis N J 1995 *Bistatic Radar* (Raleigh, NC: Scitech)
[108] Willis N J and Griffiths H D 2007 *Advances in Bistatic Radar* (Raleigh, NC: Scitech)
[109] Woodward P M 1953 *Probability and Information Theory, with Applications to Radar* (New York: McGraw-Hill)
[110] Xiao S 2001 Topics in CT and SAR imaging: fast back-projection algorithms and optimal antenna spacings *PhD Thesis* Univ. of Illinois at Urbana-Champaign
[111] Xiao S, Munson D C, Basu S and Bresler Y 2000 An $N^2 \log N$ back-projection algorithm for SAR image formation *Proc. 34th Asilomar Conf. on Signals, Systems, and Computers* (Pacific Grove, CA, 31 Oct.–1 Nov. 2000)
[112] Yazici B, Cheney M and Yarman C E 2006 Synthetic-aperture inversion in the presence of noise and clutter *Inverse Problems* **22** 1705–29
[113] Yazici G and Xie G 2006 Wideband extended range-doppler imaging and waveform design in the presence of clutter and noise *IEEE Trans. Inf. Theory* **52** 4563–80
[114] Yarman C E and Yazici B 2008 Synthetic aperture hitchhiker imaging *IEEE Trans. Image Processing* **17** 2156–73
[115] Yarman C E, Yazici B and Cheney M 2007 Bistatic synthetic aperture hitchhiker imaging *Proc. IEEE Int. Conf. on Acoustics, Speech and Signal Processing* vol 1, pp I-537–I-540
[116] Zeemanian A H 1965 *Distribution Theory and Transform Analysis* (New York: Dover)